# Deposition of $Au_N$ clusters on Au(111) surfaces. I. Atomic-scale modeling

Q. Hou,[1,2] M. Hou,[2] L. Bardotti,[3] B. Prével,[3,*] P. Mélinon,[3] and A. Perez[3]
[1]*Key Laboratory of Radiation Physics and Technology, Institute of Nuclear Science and Technology, Sichuan University, Chengdu 610064, People's Republic of China*
[2]*Physique des Solides Irradiés CP234, Université Libre de Bruxelles, Bd du Triomphe, B-1050 Brussels, Belgium*
[3]*Département de Physique des Matériaux, Université Claude Bernard, Lyon I, 43 Bd du 11 Novembre 1918, Villeurbanne Cédex, France*
(Received 19 October 1999)

The interaction between a monokinetic and mass resolved low-energy gold cluster beam and a gold (111) surface is studied in detail at room temperature by means of molecular dynamics. The model makes use of the classical second moment tight-binding approximation to estimate the interatomic forces. A model is described to account for the electron-phonon coupling. Clusters of the nanometer size are modeled to slow down one after the other on the gold surface until a nanostructured layer about 7 nm thick is formed. The cluster slowing down is studied in detail and the consequences of the diffusionless accumulation of clusters on the surface is investigated. The first impinging clusters undergo pronounced epitaxy with the substrate surface although defects of various kinds can take place in them. The further cluster slowing down stimulates the annihilation of these defects. A pronounced surface roughness indicates no significant coalescence. As the slowing down proceeds further, cluster layers become increasingly defective and highly stressed. This stress field propagates into the first cluster layer, inducing lattice distortions. The memory of the surface orientation is progressively lost as the deposited layer thickness increases. The cluster assembled is characterized by numerous cavities of the nanometer size that may be interconnected and form nanopores. Incident conditions are found to play an important role, which motivates a realistic comparison between simulated and real experiments.

## I. INTRODUCTION

Nanostructured materials represent a class of solids formed by structural elements of a few nanometer size with specific properties governed by the nature of these elements. Most of these properties are still not well known and stimulate a huge and growing interest. Although such materials can be synthesized for more than two decades by means of a wide range of methods (see, for instance, Refs. 1–5), their systematic fundamental study is quite recent.

Because of the lack of periodicity, the accurate experimental characterization of such systems is unfortunately an arduous task and therefore, atomic scale modelling represents a useful method for predictions beyond the limit of presently available experimental capabilities. The effort achieved in this direction is quite substantial.[6–12] Simulated nanostructured materials (NsMs) are constructed in different ways. NsMs deformation mechanisms are discussed in Ref. 6, and film growth is studied in Ref. 7 by modeling the cluster accumulation on a substrate surface by energetic slowing down. The compacting of initially adjacent clusters is simulated in Ref. 10. In Refs. 8 and 9, crystals are grown on geometrical lattices from seeds randomly distributed and oriented in space until space filling is obtained. A similar method is used in Refs. 11 and 12 according to which crystal seeds are embedded into a melt that crystallizes into some nanostructured system. The simulated interfaces can then be analyzed in detail as well as their response to external mechanical constraints.[8,9,13] Since none of these modeling methods exactly reproduce the experimental synthesis techniques, the sensitivity of the obtained NsMs models on the construction methods needs thorough investigation. On the other hand, since classical atomic scale models are partially empirical, there is a need for a support by experimental facts before to allow predictions beyond the limit of the experimental observation possibilities. One of the currently used technique is the low-energy cluster beam deposition (LECBD) method.[14] The mesoscopic modelling of such deposited metallic cluster aggregation by means of cluster diffusion is achieved in Refs. 15 and 16, which very nicely reproduce the experimentally observed diffusion patterns. The detail of the interatomic interactions is not accounted for so far and the method does not allow predictions about the atomic accommodation at the cluster interfaces. Classical molecular dynamics (MD) with a simple Lennard-Jones potential allowed us to identify the conditions for cluster diffusion.[17] The importance of the lattice-parameter mismatch between the substrate surface and the cluster is emphasized and no significant diffusion is predicted in the case of good lattice-parameter matching. This particular case was specifically considered in Ref. 18 with a realistic semiempirical potential.

The present paper is part of a program, which aims at developing a method that combines experiment and atomic scale modeling for understanding the growth and the properties of nanostructured films formed by deposition without the contribution of cluster diffusion. This paper emphasizes the modeling method and predictions are made about NsM characteristics, which can be expected in a real experiment. These are useful to set up the NsM study combining simulated and real experiments. The conclusions reached with such a combination will be presented in a distinct paper.[19]

The size of clusters produced by LECBD is typically of 1 to 5 nm, which represents a few hundred to a few thousand

 

atoms. Apart from the interactions between clusters and substrate, the interactions between deposited clusters could also play an important role in the morphology of cluster-assembled films. In the present paper, we focus on the interaction between the clusters and the substrate on which they are deposited and the interaction between the clusters themselves during the deposition process. We also consider the memory of the substrate ordering on the structure of the overlayer and some properties of this overlayer as compared to those of macroscopic bulk materials.

We simulate the deposition and assembling of identical Au clusters formed by a few hundred atoms on an Au (111) single-crystal surface. This way, no significant lattice mismatch between the clusters and the substrate is expected and cluster diffusion is discarded. The simulations of the deposition and assembling for large clusters (containing a few hundred atoms or more) was first given in Refs. 20 and 21 where the simulations are carried out for a two-dimensional system with Lennard-Jones interactions. In Ref. 7, this modeling technique was extended to three-dimensional systems with a realistic interaction model. The authors investigated the slowing down of Mo clusters containing about thousand atoms on a Mo (001) surface with deposition energies from 0.1 to 10.0 eV/atom. This study was achieved by classical molecular dynamics. An overall examination of the results shows that in the softest landing case, the clusters are loosely stacked together without significant change in their morphology and voids remain between them. In the highest-energy case, which is way above typical LECBD energies, the clusters form a dense epitaxial film, partially buried in the substrate. In a later work,[18] and already in view of studying LECBD conditions, the detail of the deposition of a single Cu cluster containing 440 atoms on a Cu (001) surface with LECBD incident energies and at different temperatures was investigated with a similar method. The main issues are the epitaxy of the cluster with the substrate and the dependence of its morphology on the deposition energy. The epitaxy of small metallic nanoclusters on single-crystal surfaces was already observed by high-resolution transmission electron microscopy.[22]

In the present paper we concentrate on the deposition and the formation of cluster-assembled gold layers by means of deposition of gold clusters, one after the other, until a thick cluster layer is obtained. We simulate the deposition of clusters containing 440 atoms with an impact energy of 0.25 eV/atom. The cluster layer growing process conditions will be discussed in detail.

In Sec. II, we give a description on the adopted simulation model, with special emphasis on the electron-phonon coupling. The results are discussed in Sec. III. A comprehensive picture of a nanostructured film growth is given in Sec. IV, and the conditions to be met for realistic comparison with experiment are briefly discussed.

## II. MODEL AND SIMULATION

The model gold clusters considered here contain a few hundred atoms each, which is a typical size of clusters in LECBD experiments. The simulated substrate should be large enough to model a semi-infinite solid. The classical MD method with a semiempirical potential to describe the interaction between atoms is nowadays the only practicable method to simulate a system that consists of a few thousands or more atoms, as needed in the present study.

### A. The model

It is well known that the atomic trajectories in a MD simulation strongly depend on the interaction potentials. It is also well known, as already predicted by the Friedel theory of transition metals, that the many-body nature of the atomic interactions need to be accounted for in order to correctly describe the interaction between atoms in materials. To this purpose, a many-body potential based on the second moment approximation of the Friedel tight-binding theory (TB) is suggested in Ref. 23 and later in Ref. 24. As an alternative, an embedded atom model (EAM) was developed for metals,[25,26] based on the local density-functional theory. Although based on different physical grounds, both the EAM and TB cohesion models may be expressed in similar mathematical forms, namely, a sum of pairwise interactions and a sum of many-body noncumulative contributions. The cohesive energy projected onto one atom can then be written as

$$E_i = F(\rho_i) + \frac{1}{2}\sum_{j\neq i} \varphi(r_{ij}), \tag{1}$$

where $F(\rho_i)$ is an $N$-body function of the electronic density $\rho_i$ on atom $i$ and $\varphi(r_{ij})$ is the repulsive energy between atoms $i$ and $j$ separated by the distance $r_{ij}$. The total cohesive energy of the system is

$$E_T = \sum_{i=1}^{N} E_i . \tag{2}$$

Many empirical potentials in this form have been generated by fitting experimental measurements of elastic constants, vacancy formation energies, etc. They are commonly applied to describe properties of bulk and surface of metals. In the present paper, we adopt the Fermi surface type potential given in Ref. 27. Because of its semiempirical nature, this potential does not perfectly and systematically reproduce all properties different from those used to adjust its free parameters. For instance, the short range usually employed does not allow a correct description of some planar extended defects in periodic crystals.[28] This is an obvious drawback of all semiempirical potentials, which is however not crucial for qualitative or generic predictions. It is thus not expected to imperil the present paper.

Other aspects of the cluster-surface interaction problem need to be accounted for with some care and one here considers the incorporation of the electron-phonon coupling in the MD model. Indeed, two factors should be considered in the heating up of the system, subsequent to the impact of a cluster on a substrate. First, the cluster will transfer its translation energy to the substrate and directly contributes to the thermalization of the ionic system. Second, when the system evolves toward thermodynamic equilibrium, the ionic system couples with the electron gas and both systems exchange energy according to the electron-phonon interaction dynamics. Because of high-thermal conductivity of the electron gas in metals, the energy transferred to the electron system is quickly dispersed. Femstosecond laser spectroscopy showed

this dispersion characteristic time to be of the order of 0.5 ps.[29] Since the evolution of a cluster impinging on a semi-infinite system toward thermodynamic equilibrium is of the order of 100 ps, the electron gas can be considered as a thermostat at constant temperature.

MD methods in the canonical ensemble are well established and commonly make use of the so-called extended system method. In this line, an additional degree of freedom to a Hamiltonian system is introduced,[30] which governs the dynamics of the exchange of energy between the system and an external thermal bath. An inertial factor controls the rate of energy exchange at constant volume. Similarly, the volume can be considered as an isotropic dynamic parameter[31] in order to describe the evolution of a system at constant external pressure. This method was generalized to any deformation of the simulation box.[32] Both methods at constant volume and at constant pressure are formally demonstrated to describe the partition function of an equilibrium canonical statistical ensemble.[30] The direct application to the dynamic evolution of a nonequilibrium system toward thermodynamic equilibrium is however not realistic provided a physical understanding of the inertial factors introduced can be given, which is still an open question. Therefore, the Langevin equation of motion has been used to model the evolution of a solid system initiated by a cascade of ballistic atomic collisions.[33,34] The stochastic Langevin force is used to describe the electron-phonon interaction explicitly at the atomic scale, which depends on the local electronic density, similarly to the embedded atom methods for interatomic forces. A simple approximate functional dependence on the electronic density is suggested in Ref. 33 for copper and compared to density-functional and Hartree-Fock estimates. This procedure is empirical and needs to be repeated for each different system.

An alternative approach is suggested in Ref. 35, which is briefly outlined here and extended on the basis of the Sommerfeld theory of metals to be used in the present cluster-surface interaction study. In this model, two coupled macroscopic nonlinear heat transport equations describing the time evolution of the electronic and the ionic temperatures model the electron-phonon interaction. This system reduces to one single equation with the simplifying assumption that the electronic temperature is constant. In this case, the equation for the rate of change of the ionic temperature is

$$\frac{dT_i(t)}{dt} = -\alpha[T_i(t) - T_e], \tag{3}$$

where $\alpha$ is the inverse of the characteristic cooling time, and $T_i$ and $T_e$ are the temperature of the atoms and electrons, respectively. Notice that this equation applies to the instantaneous temperature of atom $i$ and it thus can be used for atomic scale modeling.

Considering that a damping force can describe the electron-phonon energy exchange through small electron-atom energy transfers,[35] this damping force on an atom $i$ can be written as

$$\mathbf{F}_i = -\mu v_i. \tag{4}$$

Then, the rate of change of thermal energy may be expressed by

$$\mathbf{F}_i \mathbf{v}_i = -\mu \mathbf{v}_i \cdot \mathbf{v}_i = \frac{\partial}{\partial t}(3k_B T_i). \tag{5}$$

According to Eq. (3),

$$\mu \mathbf{v}_i \cdot \mathbf{v}_i = 3k_B \alpha[T_i(t) - T_e]$$

and since $T_i = mv_i^2/3k_B$, or $v_i^2 = (3k_B/m)T_i$, we have

$$\mu = m\alpha \frac{(T_i - T_e)}{T_i}. \tag{6}$$

In this model, the motion of atom $i$ is thus governed by the equation

$$\frac{d^2\mathbf{r}_i}{dt^2} = \frac{1}{m_i}\nabla_{\mathbf{r}_i} E_T - \mu \mathbf{v}_i. \tag{7}$$

This equation is similar to the Nosé equation of motion in the form written by Hoover.[36] Therefore, we think it describes the evolution of a system toward thermodynamic equilibrium in the canonical ensemble. It introduces a relationship between electron-phonon coupling and the inertial parameter introduced by Nosé, which will not be discussed in the present paper.

As shown in the appendix, the Sommerfeld theory for metals allows writing down the inverse of the electron-phonon coupling time $\alpha$ as

$$\alpha = \frac{\Theta_D T_e L n e^2 k_B Z}{2 m_e \kappa \varepsilon_F}, \tag{8}$$

where $\Theta_D$ is the Debye temperature, $k_B$ the Botlzmann constant, $L$ the Lorentz number, $n$ the density of electrons, $Z$ the valence, $\kappa$ the thermal conductivity, $\varepsilon_F$ the Fermi energy, and $e$ and $m_e$ the electron charge and mass, respectively. In this expression, all quantities are available and none is much temperature dependent. Using the experimental value of the Lorentz number, the characteristic time $\alpha^{-1}$ for Au is about 20 ps at room temperature.

Equation (5) is integrated numerically by the scheme proposed by Swope *et al.*[37] The force evaluation makes use of Verlet neighbor lists combined with a linked cell algorithm. The potential cutoff distance selected is given in Ref. 27 and includes third neighbors for fcc metals.

### B. The simulation conditions

We consider the deposition of gold clusters formed by 440 atoms on a fcc (111) gold surface. The substrate is 12 monolayers thick and each layer contains $18 \times 20$ atomic cells. Thus, the size of initial substrate box is a $18a_x \times 20a_y \times 12a_z$ parallelepiped, where

$$a_x = \frac{\sqrt{2}}{2} a_0,$$

$$a_y = \frac{\sqrt{6}}{4} a_0,$$

and

$$a_z = \frac{\sqrt{3}}{3} a_0$$

with $a_0$ being the gold lattice parameter. Such a surface area is of the same order as the perfect fcc domains observed in reconstructed Au(111) surfaces at room temperature.[38] The effect of boundaries between faulted and unfaulted areas is not considered. Born von Karman periodic boundary conditions are applied in the $x$ and $y$ directions, parallel to the (111) surface plane. Before simulating the deposition processes, the substrate is prepared by relaxation at room temperature (300 K).

Each cluster is constructed by cutting a sphere out of a fcc box. No particular attention is paid to the initial cluster morphology, which is unknown in the gas phase. It is hoped that an equilibrium morphology is found by a heating and cooling cycle before thermalization at 300 K. The possible role of the cluster morphology on deposition will be addressed in another study. Before starting the dynamics of the cluster-surface interaction, the cluster is rotated at random around its center-of-mass and positioned at random in the $x$-$y$ plane [the plane parallel to the (111) surface]. The $z$ coordinate above the surface is selected to warrant a distance between the nearest atom in the cluster and the topmost atom in the surface to be just smaller than the interaction cutoff distance substrate (the previously deposited clusters are accounted for). The cluster is then set to its initial translation velocity. For each cluster, the simulated process lasts for 200 ps and the equilibrium is checked by controlling the time evolution of the temperature and the configuration energy. Then, a next run begins for a next cluster and so on, until a thick nanostructured layer is formed.

The use of periodic boundary conditions allows energy to artificially propagate back to where it comes from and this can be avoided, e.g., by applying suitable applied stochastic forces in selected box areas. In the present case however, the impact energy is small enough and the surface area sufficiently large that such a precaution is not found necessary. It is well known however that the impact of a heavy particle on a solid induces a compressive wave that propagates across the substrate. The reflection of this wave at the boundaries of the finite simulation box is undesirable and this one needs to be presently avoided. The problem is addressed in Ref. 39 and was recently revisited in Ref. 40 where a damping method is suggested using spherical symmetry to separate the zone of interest from a harmonic system with an efficient damping interface. We notice that, in the case of small impact energies, an efficient reduction of the reflection amplitude could also be obtained by applying Eq. (4) with a short-time damping force to the atoms in a plane layer in the bottom of the simulation box. The time this artificial damping is applied is long enough for the compressive wave to reach the bottom of the box, but short enough to prevent any interference with the cluster-surface interaction process.

## III. RESULTS

For the convenience of discussion, we subdivide the detailed results into four sections.

### A. Deposition of a first cluster

We here provide details about the impact of the first cluster of 440 atoms on the gold surface at 300 K. The initial translation energy of the incident cluster is 0.25 eV per atom.

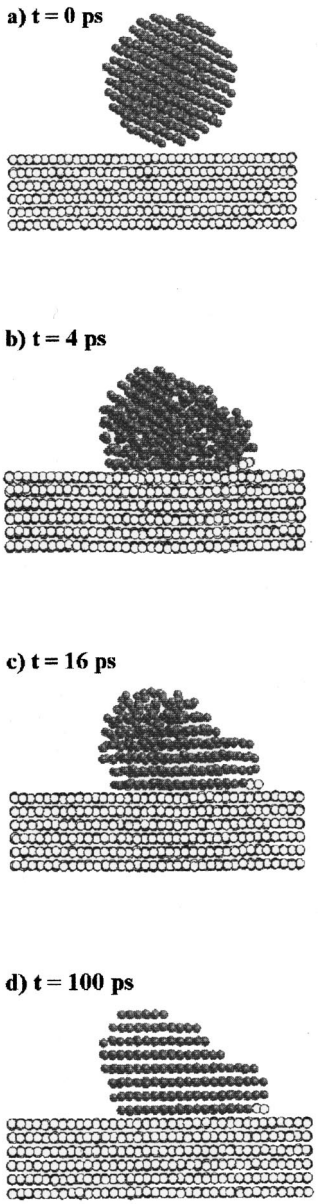


FIG. 1. Snapshots of the deposition of a Au cluster containing 440 atoms on a Au(111) surface. The cluster is initially positioned in such a way that a distance close to the potential cutoff separates the closest cluster atom from the surface. At $t = 100$ ps, the cluster is fully epitaxial to the surface.

The compressive wave mentioned above is formed within the first picosecond and it disappears by the combined effect of thermal dispersion and the damping applied in the bottom of the simulation box, within a delay of the order of 2 ps. This is one order of magnitude shorter than the characteristic electron-phonon coupling time.

Figure 1 displays four snapshots illustrative of the dynamics of the interaction between the first cluster and the substrate. The initial cluster is crashed onto the surface within a simulation time shorter than 4 ps, along which process, some mixing between the cluster and the substrate takes place. The number of exchanges represents no more than 1% of the number of the cluster atoms. This exchange rate is also observed when the slowing down is repeated with different random initial orientations and positions of the cluster. No

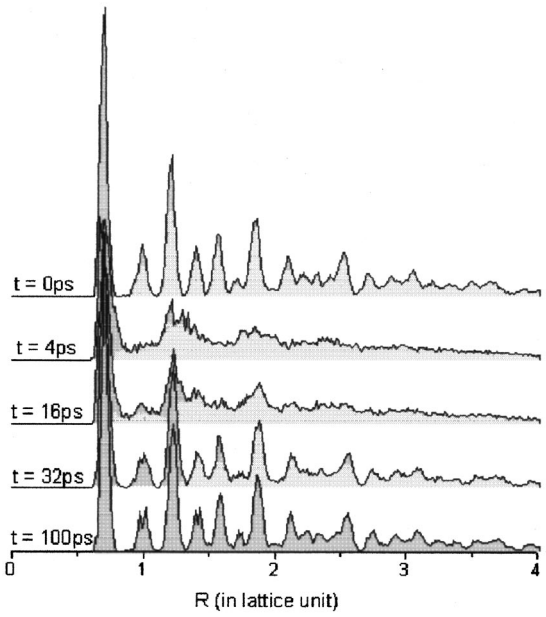


FIG. 2. The pair correlation functions at different cluster-substrate interaction times. At $t=4$ ps, the disappearing of the second neighbor peak in the pair-correlation function shows that the short-range order is destroyed. At $t=16$ ps, the second peak appears again, showing that the order is partially restored. At $t=32$ ps the cluster structure is almost fully recovered.

later exchange is observed and mixing is thus a minor short-term effect. At $t=4$ ps, the initial structure of the cluster is destroyed. This is verified by an examination of the (nonnormalized) radial pair-correlation function in the cluster, measured as a function of time and displayed in Fig. 2. Indeed, at $t=4$ ps, the second peak of the correlation function has completely disappeared. At $t=16$ ps, this second peak starts to restore and the process is completed at $t=32$ ps. After $t=10$ ps, the epitaxy starts from the cluster-substrate interface and quickly propagates across the cluster. Figure 1(c) shows an intermediate state at $t=16$ ps where a defect remains. This one is annealed at $t=32$ ps, as it comes out of the pair-correlation function in Fig. 2. It is found (snapshots not shown here) that between $t=32$ ps and $t=100$ ps, the system still evolves as the atoms exchanged with the substrate undergo further site exchanges. This indicates the occurrence of diffusion jumps in the cluster, while altering neither its overall morphology nor its pair-correlation function. Facets characteristic of its final morphology can be noticed in Fig. 1(d), consistently with similar simulations performed in the case of copper.[18] It is predicted in Ref. 41 that a tiny gold tip (containing less atoms than our model cluster) deposited on a gold (111) surface, collapses at 800 K within a time interval of several hundred pico seconds. This is not observed in the present case because the average temperature used is 300 K and the electron-phonon coupling moderates the duration of the local heating.

The kinetic evolution of the system toward thermodynamic equilibrium is governed by the characteristic electron-phonon coupling time. In a first step, the conversion of the initial cluster kinetic energy into potential energy occurs within a few picoseconds. The result of this step corresponds to the configuration in Fig. 1(b). This potential energy is then converted into heat in the ionic system, which then exponentially cools down, with the characteristic time of the electron-phonon coupling, simultaneously with a decrease of the mean configuration energy, toward thermodynamic equilibrium. The electron-phonon time constant is 20 ps at 300 K and, consequently, equilibrium is only reached at times larger than 100 ps. This is the reason why the simulation time for each slowing down lasts 200 ps in the present paper.

### B. Deposition of the second cluster

Figure 3 exhibits snapshots of the deposition of the second cluster. The first cluster has the configuration shown in Fig. 1(d) and the second, initialized as described above, turns out to be positioned in the vicinity of the first. Before hitting the substrate, this cluster undergoes a slight impact from the first deposited cluster, as shown in Fig. 3(a). This impact causes a local compression of both clusters. Some minor mixing takes place. Since the second cluster interacts with the first cluster before reaching the surface, no significant compression wave propagates into the substrate. In addition, no mixing with the substrate is observed. In the later stages, epitaxy is observed to progress from the interfaces with the substrate [snapshot in Fig. 3(b)] and with the first cluster [snapshot in Fig. 3(c)]. The snapshots are selected at $t=16$ ps and $t=32$ ps, respectively. At the end of this run, the epitaxy is not as perfect as that for the first cluster. In contrast with the first slowing down, disorder remains and the second cluster is not fully epitaxial [Fig. 3(d)]. Planar defects like stacking faults or twin boundaries are found in other cases as well. As will be shown below, such defects can be annihilated by the impact of further coming clusters.

### C. Deposition of the first cluster layer

More clusters can be accumulated the same way and Fig. 4 shows the morphology of the first cluster layer at equilibrium, viewed in a $[\bar{1}10]$ direction. The clusters are all fully epitaxial to the substrate. The defect in the second cluster shown in Fig. 3 is annihilated. It is observed that when a cluster slows down in the vicinity of another one, which is defective, the energy transferred either directly or via the substrate is sufficient to overcome the energy barrier for annihilation. The effect is enhanced by the fact that epitaxy not only originates from the substrate but also from the neighboring clusters. One question often addressed is that of the possible cluster coalescence during the slowing down process. The top view of the first cluster layer [Fig. 4(b)] clearly shows that the clusters keep their identity. They display a pronounced tendency of well-defined facets for which relative orientations are governed by the crystallography. Cavities between the clusters remain. This is qualitatively consistent with the simulation of heterogeneous cluster-substrate systems presented in Refs. 41 and 42 where a similar layer growth mechanism is found and where it is shown that high temperatures are necessary to induce the cluster collapse. The coalescence of free gold clusters was also predicted at high temperature, though below the melting point.[43]

We have also investigated the inner structure of the first cluster layer by observing the sample in Fig. 4(a) slice-by-slice. Figure 4(c) is one of such $[\bar{1}10]$ slice and Fig. 4(d) is

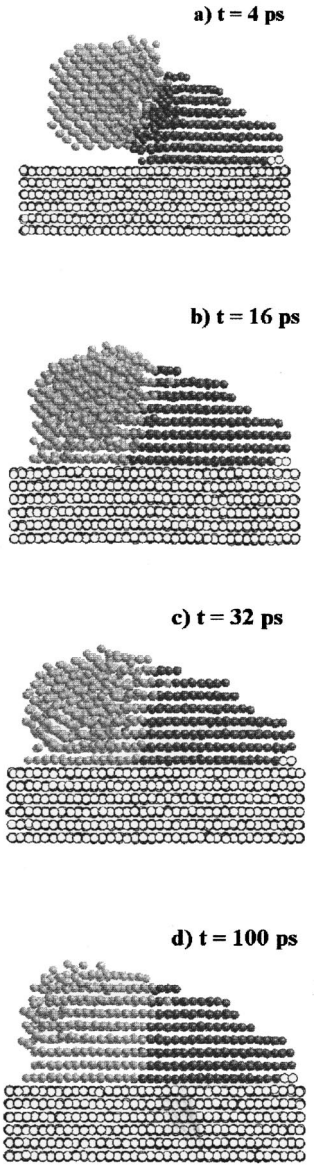


FIG. 3. Snapshots of the deposition of a second cluster. The initial configuration for this slowing down is not shown. This second cluster has a slight impact with the first cluster. At $t = 16$ ps, the cluster starts to become epitaxial with the substrate and, at $t = 32$ ps, with the first cluster. A defect is still remaining at $t = 100$ ps, which will not be annihilated before the end of the simulation time.

a slice selected in the cluster layer along the [111] direction, parallel to the substrate surface. Both illustrate the occurrence of cavities with size on the same order as that of the clusters themselves. Atoms of a later coming cluster may however fill spaces left empty by the previously deposited ones, hence tending to make this first cluster layer somewhat more compact than a stacking of hard spheres would be. An animation of the process shows that such a filling happens during impact stage, that is, before the epitaxial ordering starts. The pronounced roughness of the surface of this first layer should be noticed [Figs. 4(a) and 4(c)], with a characteristic length of the order of the cluster diameter. As will be shown below, this roughness is a determinant in the deposition process of the next cluster layer and the overall state of

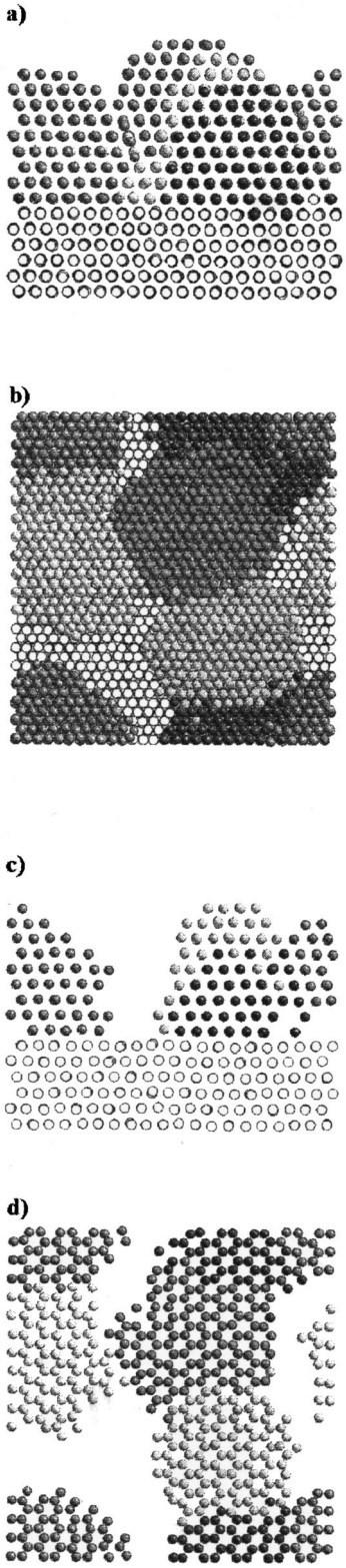


FIG. 4. The first cluster layer, as formed by the five clusters. These clusters are fully epitaxial with the substrate. The clusters keep their distinguishable shape and no obvious coalescence is observed. (a) View in the $[\bar{1}10]$ direction, (b) view in the [111] direction, (c) and (d) are slices in (a) and (b), respectively. Their thickness is of one monolayer.

a thick cluster assembled layer grown by low-energy cluster beam deposition.

### D. Deposition of a thick cluster layer and equilibrium structural properties

After the first cluster layer shown in Fig. 4 is formed, the cavities left are too small to allow the further deposited clusters to come into direct contact with the substrate surface. Owing to the model geometry, five clusters were enough to form the first cluster layer. A second layer was formed of seven additional clusters. The roughness of the nanostructured cluster surface formed makes the definition of a cluster layer inaccurate. Here we define the first layer as formed by the first five clusters because they are in direct contact with the substrate. The second layer is defined for convenience as formed by the clusters in direct contact with those in the first, but not with the substrate, and so on.

The clusters in the second layer also undergo epitaxy without any impact induced coalescence. By visualizing the deposition processes (not displayed here), it is observed, just as in the case of the first layer deposition, that in a first step, the second cluster layer structure is heavily damaged. The final structure of this layer is not influenced by the perfect substrate surface, but by the rough surface of the first layer. This represents a major difference with the first layer deposition and the epitaxy of the second layer is only partial. The defects induced by the impact are no more fully annihilated. As the deposition proceeds, the memory of the substrate surface becomes increasingly loose and the nanostructure becomes dominantly governed by the cluster-cluster interaction.

Clusters are deposited further at time intervals of 200 ps until a film is formed containing 20 clusters. Its total thickness is about 7 nm. The deposition of the third layer modifies the structure of the second for which epitaxy is still further decreased. As a result, major rearrangement takes place, which is now described.

This 7-nm-thick nanostructured layer is formed by nanocrystal grains separated by interfaces for which spatial extension has no straightforward relation with the size of the initial clusters. In addition, the clusters deposited after the first cluster layer do not fill the empty spaces left in it. The former deposited clusters support them and, like the preceding ones, they leave cavities of the nanometer size. Figure 5 displays a typical slice in this nanostructured layer. Large holes are clearly observed. Lattice distortion is observed too, which is commented below.

Our simulated sample is too small to allow a statistical study of the grains. Specific features however can be clearly identified, which are now discussed. The large holes observed in Fig. 5 may interconnect to form pores that cross most of the sample thickness. The slice in Fig. 5 displays no other lattice defects than an edge dislocation for which the line is located in the plane marked by an arrow. This demonstrates that at least a partial memory of the substrate ordering is maintained across the whole layer. Further examination of this model sample reveals strong three-dimensional lattice distortions and other extended defects like twin grain boundaries and stacking faults, which are not shown here. The nanostructure is thus highly complex and will not be analyzed in detail. Overall trends may be better emphasized

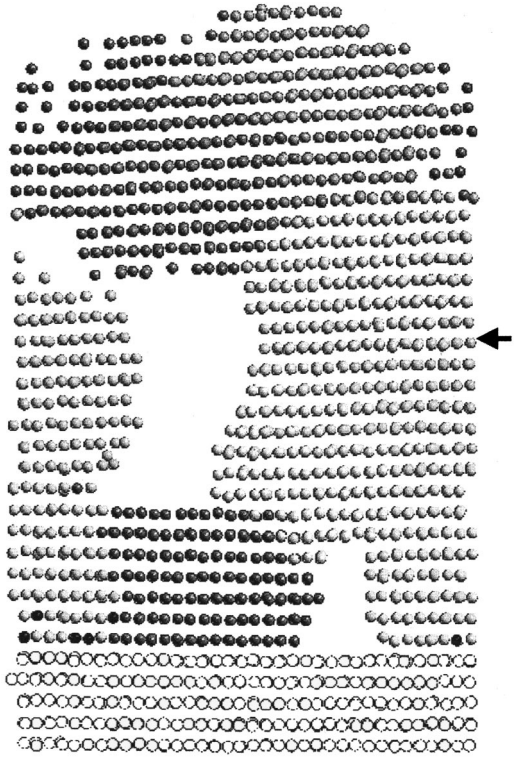

FIG. 5. A one monolayer slabs in the thick nanoclustered film formed by 20 clusters viewed in the $[11\bar{2}]$ direction. The arrow points to the core of an edge dislocation, parallel to the substrate surface.

with the help of an order parameter and we use the structure factor $S(\mathbf{k})$ the same way as in Ref. 18. $S(\mathbf{k})$ provides better quantitative information than visualization. It is here defined as

$$S(\mathbf{k}) = \frac{1}{N}\sum_{i=1}^{N} \exp(i\mathbf{k}\cdot\mathbf{r}_i),$$

where $N$ is the number of atoms concerned, $\mathbf{k}$ is the wave vector defined for convenience by

$$\mathbf{k} = \frac{4\pi}{a}(n_x, n_y, n_z)$$

with $a$ being lattice parameter and $(n_x, n_y, n_z)$ the Miller indices. With this definition, the square modulus, $|S(\mathbf{k})|^2$, of a perfect fcc crystal is equal to one in the case of full order and to zero in case of full disorder. For the cluster layer, we use $\mathbf{k}$ parallel to low index directions in the substrate in such a way that $|S(\mathbf{k})|^2$ provides a quantitative measure of direction correlations between the substrate and the deposited layer. Much of the information discussed above can be retrieved by a detailed analysis of the structure factor, which will not be presented here. We limit ourselves to the measure of the memory of the substrate ordering in each deposited cluster.

One example of the evolution of the structure factor measured in given clusters as a function of the number of further deposited clusters is given in Fig. 6. This figure represents the structure factor with $\mathbf{k}$ parallel to $[\bar{1}10]$, associated to a given cluster as a function of the number of further deposited

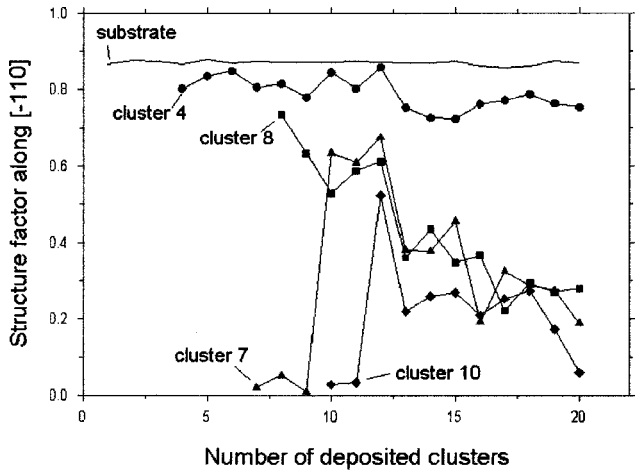


FIG. 6. The structure factor associated to individual clusters (**k** vector parallel to the substrate $[\bar{1}10]$ direction) as a function of the number of deposited clusters. Clusters are numbered from 1 to 20 according to the deposition sequence. Each impact modifies the structure factor associated to the formerly deposited clusters. This figure represents the structure factor measured in fourth, seventh, eighth, and ninth deposited clusters as a function of the further deposited ones. Its value in the substrate is also shown. The substrate and the fourth deposited cluster (sitting in the first cluster layer) keep high constant structure factor values. The structure factor associated to the seventh deposited cluster is initially small and is enhanced by the impact of the tenth cluster for which the structure factor value is on its turn enhanced by the slowing down of the twelfth cluster. This enhancement effect competes with damage, also resulting from further cluster deposition.

clusters. Several features are coming out. For instance, the structure factor associated to the seventh deposited cluster is enhanced because of the deposition of the tenth cluster. This shows that the tenth cluster impact makes the seventh cluster epitaxial. The further slowing down, as commented above, then progressively deteriorates this epitaxy. A similar phenomenon of sudden epitaxy enhancement followed by its progressive deterioration is systematically observed for the later deposited clusters. Epitaxy becomes progressively loose as the layer thickness increases, except in the first layer in which the structure factor remains close to constant as the slowing down proceeds, because of the substrate. This is shown in Fig. 6 on the example of the fourth deposited cluster. The substrate remains undamaged.

These observations displayed in the case of a **k** vector parallel to $[\bar{1}10]$ are found for all other considered **k** vectors and are cross checked by an examination of the density function measured normal to the substrate surface, which is shown in Fig. 7. This figure shows that the atomic layer structure becomes increasingly loose as the thickness is increased. A decrease of the peak height is observed, balanced by broadening, in the vicinity of the substrate surface. This illustrates interface relaxation, which turns out to be short range in the substrate, related to an enhancement of thermal vibration amplitudes. A close comparison of the peak integrals, providing the layer-by-layer density, demonstrates, in relation with the holes commented above, that the nanostructured layer density is not significantly depth dependent and is somewhat less then 80% of the substrate density. This is to be compared with the density of 0.52 that should be obtained

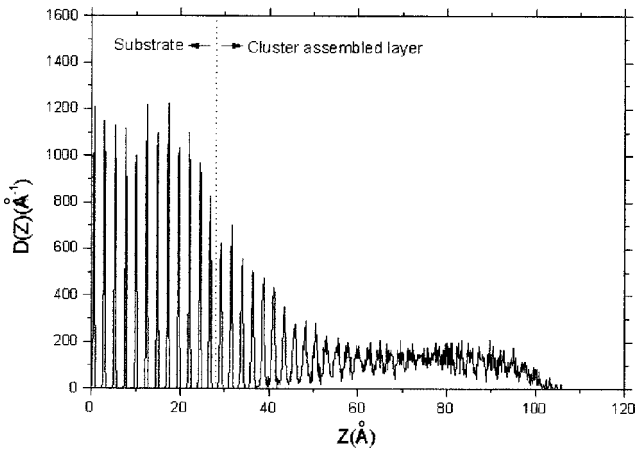


FIG. 7. The atomic density distribution function, $D(z)$, measured along the [111] direction perpendicular to the substrate surface ($z$ direction in the figure). The first 12 peaks correspond to substrate monolayers.

for a compact staking of hard spheres. The peaks in the cluster layer are quite broad, illustrating the distortions mentioned above and the layer structure vanishes close to the surface. This one is characterized by a smooth tail, which illustrates its roughness.

## IV. CONCLUDING REMARKS

At this stage, it becomes possible to provide a comprehensive, though qualitative, description of metallic nanostructured diffusionless film growth.

When a gold cluster of the nanometer size impinges on a crystalline gold surface at low energy in an otherwise isolated environment, it becomes pronouncedly epitaxial with the substrate. The time required to reach thermodynamic equilibrium is determined by the electron-phonon coupling time which is, according to the Sommerfeld model of metals, about 20 ps for gold at room temperature. The epitaxy starts at the cluster-substrate interface and quickly propagates through the cluster. In the present paper, 200 ps system evolution is necessary for each cluster slowing down in order to reach thermodynamic equilibrium. Clusters are deposited one-by-one and when the deposited dose is large enough, further incident clusters interact with both the substrate surface and the already deposited clusters. Their impact may be sufficient to annihilate existing defects and their own epitaxy is induced by both the substrate surface and the already deposited epitaxial clusters. This way, a perfectly epitaxial cluster monolayer can be formed, which is however characterized by nanosize cavities between them, the absence of coalescence and a rough monolayer surface. This roughness inhibits the epitaxy of later incident clusters, as it tends to promote defect formation. Clusters in this forming overlayer are thus less stable than those in contact with the substrate and they tend to loose their identity by interacting together. Deep rearrangement progressively takes place leaving dislocations, stacking faults, and twin boundaries in the film. The overlayer is consequently stressed and the stressed field propagates inside the first cluster monolayer inducing strong lattice distortions. Large cavities are distributed through the whole film, which may interconnect. The nanostructured

layer surface roughness seems independent on the layer thickness but it is characteristic of the cluster size. In the presently modeled experiment, because of the occurrence of cavities, the nanostructured layer density is no more than 80% of bulk single-crystal gold. The interaction between the clusters makes this density larger than that of a compact stacking of hard spheres.

It was shown in Ref. 18 that, within an energy range between 0 and 1 eV per atom, the morphology of a deposited cluster at equilibrium depends on the incident energy. It can be expected that it is also dependent on the cluster size and the substrate temperature. Since, at room temperature, their size and morphology determines the roughness of the surface film and that this roughness plays an important role in the further film growth, size and energy are obviously important parameters determining the nanostructures. In a real low energy (neutral) cluster beam deposition and film formation, the incident energy is not accurately known since it is uneasy to measure with high resolution. The mass distribution, although quite narrow as compared to other techniques, has some appreciable width. Therefore, in order to model a nanostructured film as obtained by the LECBD technique quantitatively, it is necessary to take these parameters into account. This is precisely what is done in a next step to the present paper which is reported in Ref. 19. The role of temperature as well as the mechanical properties of the films produced is the subject of further investigations.

## ACKNOWLEDGMENTS

Q. Hou is pleased to acknowledge the Université Libre de Bruxelles for the financial support and hospitality. This work was partially supported by the Belgian OSTC under Contract No. IUAP 4/10.

## APPENDIX

According to Ref. 34, let us write the electron-phonon mean-free path (mean-free path of the electrons for the scattering by ions) as

$$\lambda_e = \frac{r_0 T_0}{T_i}, \tag{A1}$$

where $r_0$ is the size of the Wigner-Seitz cell. Assuming that the number of electrons taking part in the scattering by phonons is

$$k_B T_e N(E_F), \tag{A2}$$

where $N(E_F)$ is the density-of-states at the Fermi energy, the mean-free flight time for the electron-ion scattering is then

$$\tau_{ei} = \frac{\lambda_e}{v_F} = \frac{r_0 T_0}{T_i v_F}, \tag{A3}$$

where $T_0$ is the temperature at which the mean-free flight equals the Wigner-Seitw cell radius. Consider that the mean energy exchanged in an electron-phonon collision is $k_B\Theta_D$ ($k_B$: Boltzmann constant, $\Theta_D$: Debye temperature), then the rate of energy exchange can be written as

$$R_{ex} = \frac{k_B\Theta_D k_B T_e N(E_F)}{\tau_{ei}} = \frac{k_B\Theta_D N(E_F) v_F T_i T_e}{r_0 T_0} \tag{A4}$$

and the net rate as

$$R_t = \frac{k_B\Theta_D N(E_F) v_F (T_i - T_e) T_e}{r_0 T_0}. \tag{A5}$$

Now, the energy balance for the ionic system is

$$C_i \frac{\partial T_i}{\partial t} = \kappa_i \nabla^2 T_i - R_t \quad \text{with} \quad C_i = c_i^v \rho_m, \tag{A6}$$

where $\kappa_i$ is the thermal conductivity of the ionic system, $c_i^v$ is its specific heat, and $\rho_m$ the ionic density.

In the absence of a source term ($\nabla^2 T_i = 0$), it is shown in Ref. 34 that

$$\frac{\partial T_i}{\partial t} = -\frac{3\Theta_D v_F \gamma_e}{\pi^2 r_0 c_i^v \rho_m} T_e \frac{T_i - T_e}{T_0}, \tag{A7}$$

where $\gamma_e$ is the electronic specific-heat coefficient. By combining Eq. (A7) with Eq. (A3), one obtains the inverse characteristic cooling time:

$$\alpha = \frac{3\Theta_D \gamma_e T_e v_F}{\pi^2 r c_i^v \rho_m T_0}. \tag{A8}$$

In Ref. 34, $\gamma_e / T_0$ is considered as material dependent adjustable parameter, which makes the model empirical. This parameter can be fixed however within the frame of the Sommerfeld theory of metals.

According to the law of Dulong and Petit,

$$c_i^v = 3 \frac{n}{\rho_m Z} k_B, \tag{A9}$$

where $n$ is the free-electron density and $Z$ the valence. In a free-electron gas,

$$c_e^v = \gamma_e T_e \quad \text{and} \quad \gamma_e = \frac{\pi^2}{2} \frac{k_B^2}{\varepsilon_F} n. \tag{A10}$$

$T_0$ can be eliminated provided an expression is found in Eq. (A1) for $\lambda_e$. The characteristic time for electron-ion scattering may be written as

$$\tau_{ei} = \frac{m_e}{\rho_{el} n e^2} = \sigma \frac{m_e}{n e^2}, \tag{A11}$$

where $\sigma$ is the electrical conductivity. Since the Lorentz number $L$ is defined by

$$\frac{\kappa}{\sigma} = LT, \tag{A12}$$

where $\kappa$ is the thermal conductivity, and since $T = T_0$ when $\lambda = r_0$, using Eq. (A1), one gets

$$r_0 = v_F \frac{\kappa}{LT} \frac{m_e}{ne^2}$$

or

$$T_0 = \frac{v_F m_e}{rLne^2} \kappa. \tag{A13}$$

Making use of Eqs. (A9), (A10), and (A13), Eq. (A8) can be written as

$$\alpha = \frac{\Theta_D T_e L n e^2 k_B Z}{2 m_e \kappa \varepsilon_F}. \tag{A14}$$

*Corresponding author: B. Prével. E-mail: prevel@dpm.univ-lyonl.fr


[1] H. J. Fecht, E. Hellstein, Z. Fu, and W. L. Johnson, Metall. Trans. A **21**, 2333 (1990).
[2] C. C. Koch, Nanostruct. Mater. **2**, 109 (1993).
[3] J. Eckert, J. C. Holzer, C. E. Krill III, and W. L. Johnson, J. Mater. Res. **7**, 1751 (1992).
[4] H. Leiter, Prog. Mater. Sci. **32**, 223 (1989).
[5] J. Reisse, H. Frangois, J. Vanndercammen, O. Fabre, A. Kirsch-Demesmaeker, C. Maerschalk, and J.-L. Delplancke, Electrochim. Acta **39**, 37 (1994).
[6] H. Van Swijgenhoven, M. Spaczer, D. Farkas, and A. Caro, Nanostruct. Mater. **12**, 323 (1999).
[7] H. Haberland, Z. Insepov, and M. Moseler, Phys. Rev. B **51**, 11 061 (1995).
[8] H. Van Swygenhoven and A. Caro, Phys. Rev. B **58**, 11 246 (1998).
[9] H. Van Swygenhoven and A. Caro, Appl. Phys. Lett. **71**, 1652 (1997).
[10] Huilong Zhu and R. S. Averback, Mater. Sci. Technol. **204**, 96 (1995).
[11] S. R. Phillipot, D. Wolf, and H. Gleiter, J. Appl. Phys. **78**, 847 (1995).
[12] J. Wang, D. Wolf, S. R. Phillpot, and H. Gleiter, Philos. Mag. A **73**, 517 (1996).
[13] J. Schiotz, F. D. Di Tolla, and K. W. Jacobsen, Nature (London) **39**, 561 (1998).
[14] P. Mélinon, V. Paillard, V. Dupuis, A. Perez, P. Jensen, A. Hoareau, J. P. Perez, J. Tuaillon, M. Broyer, J. L. Vialle, M. Pellarin, B. Baguenard, and J. Lerme, Int. J. Mod. Phys. B **139**, 339 (1995).
[15] A. Perez, P. Mélinon, V. Dupuis, P. Jensen, B. Prével, J. Tuaillon, L. Bardotti, C. Martet, M. Treilleux, M. Broyer, M. Pellarin, J. L. Vialle, and B. Palpant, J. Phys. D **30**, 1 (1997).
[16] L. Bardotti, P. Jensen, A. Hoareau, M. Treilleux, and B. Cabaud, Phys. Rev. Lett. **74**, 4694 (1995).
[17] P. Deltour, J. L. Barrat, and P. Jensen, Phys. Rev. Lett. **78**, 4597 (1997).
[18] M. Hou, Nucl. Instrum. Methods Phys. Res. B **135**, 501 (1998).
[19] L. Bardotti, B. Prével, P. Mélinon, A. Perez, M. Hou, and Q. Hou, Phys. Rev. B (to be published).
[20] K. H. Muller, J. Appl. Phys. **61**, 2516 (1987).
[21] K. H. Muller, Phys. Rev. B **35**, 7906 (1987).
[22] S. Giorgio, H. Graoui, C. Chapon, and C. R. Henry, Cryst. Res. Technol. **33**, 1061 (1998); S. Giorgio, C. Chapon, C. R. Henry, and G. Nihoul, Philos. Mag. B **67**, 773 (1993).
[23] F. Ducastelle, J. Phys. **31**, 1055 (1970).
[24] M. W. Finnis and J. E. Sinclair, Philos. Mag. A **50**, 45 (1984).
[25] M. S. Daw and M. I. Baskes, Phys. Rev. Lett. **50**, 1285 (1983).
[26] M. S. Daw and M. I. Baskes, Phys. Rev. B **29**, 6443 (1984).
[27] G. J. Ackland and V. Vitek, Phys. Rev. B **41**, 10 324 (1990).
[28] P. Heino, L. Perondi, E. Kaski, and E. Ristolainen, Phys. Rev. B **60**, 14 625 (1999).
[29] V. Halté, B. Palpant, B. Prével, J-C. Merle, M. Broyer, A. Perez, and J-Y. Bigot, in *Ultrafast Phenomena*, edited by T. Eksaesser, J. G. Fujimoto, D. A. Wursmma, and Z. Zinth (Springer-Verlag, New York, 1998), p. 333.
[30] S. Nosé, J. Chem. Phys. **81**, 511 (1984).
[31] H. G. Andersen, J. Chem. Phys. **72**, 2384 (1980).
[32] A. Rahman and M. Parinello, J. Appl. Phys. **52**, 7182 (1981).
[33] A. Caro and M. Victoria, Phys. Rev. A **40**, 2287 (1989).
[34] C. P. Flynn and R. S. Averback, Phys. Rev. B **38**, 7118 (1988).
[35] M. W. Finnis, P. Agnew, and A. J. E. Foreman, Phys. Rev. B **44**, 567 (1991).
[36] W. G. Hoover, *Molecular Dynamics* (Springer-Verlag, New York, 1986).
[37] W. C. Swope, H. C. Anderson, P. H. Berens, and K. R. Wilson, J. Chem. Phys. **76**, 1 (1982).
[38] A. R. Sandy, S. G. J. Mochrie, D. M. Zehner, K. G. Huang, and D. Gibbs, Phys. Rev. B **43**, 4667 (1991).
[39] S. A. Aldemann and J. D. Doll, J. Chem. Phys. **64**, 2375 (1976).
[40] M. Moseler, J. Nordick, and H. Haberland, Phys. Rev. B **56**, 15 439 (1997).
[41] W. D. Luedtke and Uzi Landman, Phys. Rev. B **44**, 5970 (1991).
[42] W. D. Luedtke and Uzi Landman, Phys. Rev. Lett. **73**, 569 (1994).
[43] L. J. Lewis, P. Jensen, and J.-L. Barrat, Phys. Rev. B **56**, 2248 (1997).